LAWRENCE
LIVERMORE
NATIONAL
LABORATORY

LLNL-PROC-654537

Heat flux management via advanced magnetic divertor configurationsand divertor detachment

E. Kolemem, S. L. Allen, B. D. Bray, M. E. Fenstermacher, D. A. Humphreys, A. W. Hyatt, C. J. Lasnier, A. W. Leonard, M. A. Makowski, A. G. McLean, R. Maingi, R. Nazikian, T. W. Petrie, V. A. Soukhanovskii, E. A. Unterberg

May 16, 2014

21st International Conference on Plasma Interactions 2014
Kanazawa, Japan
May 26, 2014 through May 30, 2014

Disclaimer

LLNL-PROC-654537

Paper P1-009

Heat flux management via advanced magnetic divertor configurations and divertor detachment

E. Kolemen[a]*, S.L. Allen[b], B.D. Bray[c], M.E. Fenstermacher[b], D.A. Humphreys[c], A.W. Hyatt[c], C.J. Lasnier[b], A.W. Leonard[c], M.A. Makowski[b], A.G. McLean[b], R. Maingi[a], R. Nazikian[a], T.W. Petrie[c], V.A. Soukhanovskii[b], and E.A. Unterberg[d]

[a]*Princeton Plasma Physics Laboratory, Princeton, New Jersey 08543, USA*

[b]*Lawrence Livermore National Laboratory, Livermore, California 94550, USA*

[c]*General Atomics, PO Box 85608, San Diego, California 92186-5608 USA*

[d]*Oak Ridge National Laboratory, PO Box 2008, Oak Ridge, Tennessee 37831 USA*

Abstract

The Snowflake Divertor control and detachment control to manage the heat flux at the divertor are successfully demonstrated at DIII-D. Results of the development and implementation of these two heat flux reduction control methods are presented.

Abstract length (150 words): 36 currently

PACS:

PSI-20 Keywords:

**Corresponding and presenting author address:* E. Kolemen, 13-417, c/o General Atomics, PO Box 85608, San Diego, CA 92186-5608, USA

Corresponding and presenting author e-mail: ekolemen@pppl.gov

1. Snowflake divertor control

The present vision of the tokamak plasma-material interface is an axisymmetric magnetic X-point divertor. One approach to handling the high heat exhaust per unit area on the plasma facing components (PFCs) is to use alternative magnetic configurations. Examples of these advanced divertors are the snowflake divertor (SD), X-divertor, super X-divertor, and X-point target divertor. These configurations require active and precise control of the magnetic configuration in order to regulate the particle and heat flow.

Recent research at DIII-D focused on the SD configuration, which uses a second-order poloidal field null created by merging, or bringing close to each other, two first-order poloidal field null points (X-points) of a standard divertor configuration [1]. A poloidal cross-section of the obtained magnetic flux surfaces with a hexagonal null-point has the appearance of a snowflake. The SD geometry results in high poloidal flux expansion and a large plasma-wetted area compared to the standard divertor, which reduces peak heat flux. Also, SD has four strike points which help share the divertor power load, compared to the two-strike-point configuration.

The exact second-order null configuration is topologically unstable to variations in coil currents, which destroy the perfect alignment. This splits the double null into two first-order null X-points, and two variants of the exact configuration called snowflake-plus and snowflake-minus are often realized in steady-state, as shown in Fig. 1.

We implemented the world's first real-time SD detection and control system on DIII-D in order to stabilize this configuration. This control employs a fast real-time snowflake identification algorithm, which accurately calculates two X-points (magnetic nulls) by locally expanding the Grad-Shafranov equation in toroidal coordinates. We assume that the plasma

in the divertor region has a low beta, and the magnetic field there can be considered curl-free. Then, the equation in toroidal coordinates around the divertor is given as

$$r\frac{\partial}{\partial r}\left(\frac{1}{r}\frac{\partial \Psi}{\partial r}\right)+\frac{\partial^2 \Psi}{\partial z^2}=0 \quad . \tag{1}$$

This equation is normalized and Ψ, the magnetic flux, is expanded around the snowflake center in radial, δr, and vertical, δz, coordinates up to the third order to achieve $\Psi_{\exp}=\Psi(c_{\exp},\delta r,\delta z)$ where $c_{\exp}$ are the expansion coefficients. Solving the first two orders of the expanded Grad-Shafranov (G-S) equation yields six unknown expansion coefficients. These unknowns are solved by first choosing three points around the snowflake center and then evaluating the components of the magnetic field given as

$$B_r=-\frac{1}{r}\frac{\partial \Psi_{\exp}}{\partial \delta z} \quad , \qquad B_z=\frac{1}{r}\frac{\partial \Psi_{\exp}}{\partial \delta x} \quad , \tag{2}$$

from the real-time equilibrium reconstruction (rt-EFIT). This gives us six linear equations for the six unknown expansion coefficients. These equations are solved using Gaussian elimination. Finally, the magnetic field nulls are solved by setting $B_r=0$, $B_z=0$. This results in the location of the two X-points: $\delta r X_1 c_{\exp}$, $\delta_z X_1 c_{\exp}$, $\delta r X_2 c_{\exp}$, and $\delta_z X_2 c_{\exp}$. The resulting algorithm is a one-step (no-iteration) fast algorithm (<<1 ms) with reasonable accuracy, which has been implemented in the DIII-D Plasma Control System (PCS).

Once the locations of the two X-points are obtained, poloidal field (PF) coils are used to control the relative locations to obtain the desired SD (exact, minus, plus). At DIII-D, the F4B, F5B, F8B are the PF coils closest to the divertor and they have therefore been used to control the SD. F9B is also effective in the SD manipulation. However, in order to avoid

damage to the unprotected surfaces inside the cyropump, the strike point must be prevented from entering the cyropump gap under any possible circumstances. To satisfy this constraint without inducing any hardware or software protection, the F9B coil is set to be zero current.

The SD control algorithm calculates the distance and angle [defined in Fig. 2(a)] components of the relative positions of the two X-points in addition to the coordinates of the snowflake centroid, r_c and z_c. The values are compared to the user-requested values and the differences are filtered and fed to the control algorithm. For precise control, the effect of the change in PF coil currents, δI_{PF}, on the X-point locations is calculated. This is achieved by applying the chain rule on the snowflake parameters:

$$\frac{\partial \delta r_{X_1}}{\partial \delta I_{PF}} = \frac{\partial \delta r_{X_1}}{\partial c_{\exp}} \left(\frac{\partial c_{\exp}}{\partial B_r} \frac{\partial B_r}{\partial I_{PF}} + \frac{\partial c_{\exp}}{\partial B_z} \frac{\partial B_z}{\partial \delta I_{PF}} \right) \quad . \tag{3}$$

Here, the first two terms, $\partial \delta r_{X_1} \delta c_{\exp}$ and $\partial \delta c_{\exp} \delta B_r$, are obtained through the manipulation of the G-S expansion, as explained above. $\partial B_z \delta I_{PF}$ is found from the Green's Function of the G-S problem. This enables us to write the variation of the snowflake geometric parameter in terms of the PF coil currents as

$$\begin{bmatrix} \delta\theta \\ \delta\rho \\ \delta r_c \\ \delta z_c \end{bmatrix} = A \begin{bmatrix} \delta I_{F4B} \\ \delta I_{F5B} \\ \delta I_{F8B} \end{bmatrix} \quad . \tag{4}$$

Then, the control needed to achieve the requested snowflake configuration is obtained by taking the pseudo-inverse of this equation and multiplying it by a weighting function, W,

$$\begin{bmatrix} \delta I_{F4B} \\ \delta I_{F5B} \\ \delta I_{F8B} \end{bmatrix} = (A^T A)^{-1} A^T W \begin{bmatrix} \delta\theta \\ \delta\rho \\ \delta r_c \\ \delta z_c \end{bmatrix} \quad . \tag{5}$$

Since there are three actuators and four control parameters, the weighing function is used to define the importance of the parameters that we wish to control. Then, a Proportional-Integral-Derivative control is used to obtain the PF-coil voltage requests to the power supplies.

An example of an almost exact SD obtained with the snowflake control is shown in Fig. 2, where the SD control is turned on at 3 seconds (shown with the red line) and ρ is controlled to a few cm until the end of the shot. Note that this is within the grid resolution of the rt-EFIT. As the perfect SD is approached, broadening of the heat flux profile at the outer strike point is observed, as shown in Fig. 2(b).

This control enabled SD minus, SD plus, and exact SD formations with varying σ, the distance between the X-points normalized to the minor radius, ranging from 0.08 to 0.5 in various scenarios. SD was successfully integrated to an advanced tokamak (AT) scenario with $\beta_N = 3.0$ and $H_{98(y,2)} \cong 1.35$. The flux profile for AT scenario with the standard divertor and SD is shown in Fig. 3. We achieved a 2.5 times increase in the flux expansion and a 2.5 reduction in peak heat flux for many energy confinement times (2–3 s) without any adverse effects to the core plasma, such as confinement. The maximum allowable heat flux on plasma-facing tiles stipulate that SD will operate under radiative conditions for fusion reactors. The radiative SD regime was explored with the gas seeding. SD control was shown to be robust under partial and full detachment conditions.

2. Detachment control

Divertor "detachment", where the particle flux at the target plates drops by more than an order of magnitude, is achieved by increasing the density close to the divertor. The ITER tokamak and future fusion reactors will require detached divertor plasmas to achieve acceptable divertor target heat loads. However, it is difficult to stabilize this effect when plasmas become fully detached. The influx of impurities into the confined plasma cause high radiation levels from this region, which may result in the thermal instability of the whole plasma, known as Multi-faceted Asymmetric Radiation From the Edge (MARFE). Thus, ITER needs to operate in a state called partial-detachment under active feedback control in order to balance the need for acceptable divertor target heat loads and core stability.

We developed a new feedback control system on DIII-D to regulate and study the physics of divertor detachment. The system uses real-time electron temperature measurements from Thomson scattering, along with impurity line ratio measurement, to compute the location of the detachment front, while monitoring the core and divertor radiation measured by the bolometer diagnostic. We employed the new system to test the feasibility of envisioned ITER partial-detachment operation, using divertor Thomson measurements on DIII-D. (ITER will have a divertor Thomson with the diagnostic capability to measure as low as 1 eV [2].) This control regulates the detachment front while minimizing the effect of the detachment on the core by fixing the core density independent of the detachment control. This is achieved by a feedback control system that uses two gas valves, as shown in Fig. 4. The valve close to the strike point regulates both deuterium fuel and impurity gas injection rates to maintain the detachment front (where the plasma temperature drops to less than a few eV) at a pre-set distance from the divertor target using the real-time electron temperature measurements, and

the far-away valve keeps the core density stationary by using the interferometry measurements.

The comparison of the core and divertor density of two DIII-D L-mode shots with and without detachment control is shown in Fig. 5. The feedback algorithm increases the density at the divertor by a factor of ~5, which leads to detachment, while keeping the core density constant.

The control stabilized the detachment front fixed at the mid-distance between the strike point and the X-point throughout the shot, as shown in the 2D Thomson projection in Fig. 6. This partial detachment reduces the radiation peak from the strike point and spreads it across the detached area, as shown in Fig. 7. The new system allows the systematic study of the physics of plasma detachment and plasma-surface interactions under constant, reproducible conditions. The data from these experiments are used to test 2D models of the scrape-off-layer and divertor plasma as well as to interpret surface erosion and material migration measurements.

Acknowledgment

This work was supported in part by the US Department of Energy under DE-AC02-09CH11466, DE-AC52-07NA27344, DE-FC02-04ER54698, and DE-AC05-00OR22725. DIII-D data shown in this paper can be obtained in digital format by following the links at https://fusion.gat.com/global/D3D_DMP.

References

[1] D. Ryutov, Phys. Plasmas **14**, 064502 (2007).

[2] E. Mukhin *et al.,* J. of Instrumentation **7**, C02063 (2012).

List of Figure Captions

Fig. 1. Three plasma equilibria in DIII-D showing the exact snowflake configuration with a double null; the snowflake-minus configuration with the secondary X-point in the private flux region; and the snowflake-plus configuration with the secondary X-point in the SOL.

Fig. 2. (a) PF coils used in SD control and the definition of the SD configuration parameters. (b) Plasma controlled to almost exact SD. The SD control starts at 3000 ms. The lower panel shows the heat flux at the outer strike point (#155478).

Fig. 3. The heat flux profile at the inner and outer strike point for (a) the standard divertor double null AT and (b) the SD (-) double null AT.

Fig. 4. Sketch of the partial-detachment control system.

Fig. 5. Data showing feedback control of divertor detachment. Red—detachment feedback control on (#153816). Black — detachment control off (no divertor fueling - #153814). Top: Divertor density measured by divertor Thomson. Bottom: Line average core density.

Fig. 6. 2D Projected divertor Thomson temperature measurements for DIII-D: (a) shot without detachment control (#153814) shows no detachment, (b) shot with partial-detachment control (#153816) achieves detached cold front region, shown in purple and blue.

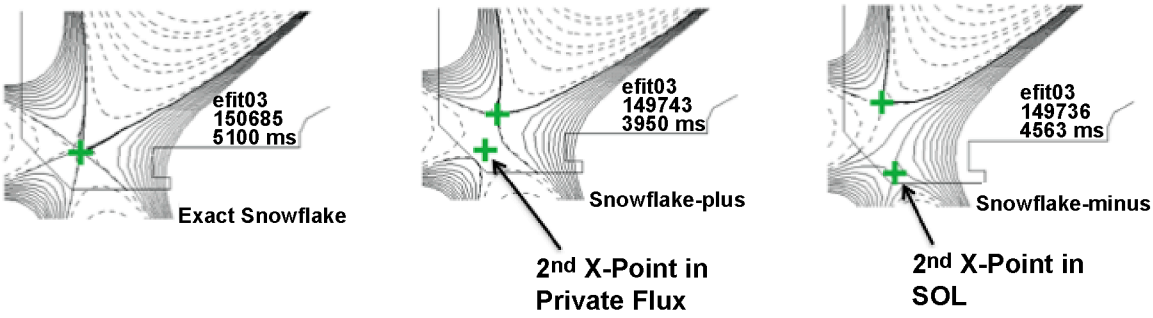
efit03
150685
5100 ms
Exact Snowflake
efit03
149743
3950 ms
Snowflake-plus
2nd X-Point in
Private Flux
efit03
149736
4563 ms
Snowflake-minus
2nd X-Point in
SOL

Fig. 1

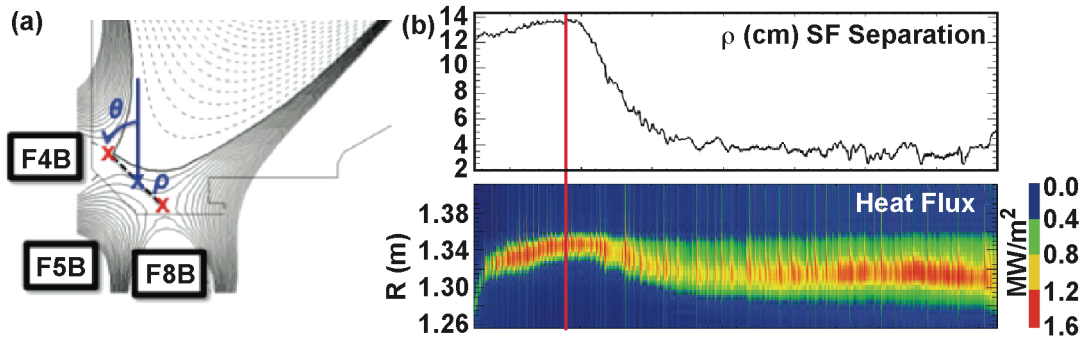
(a)
θ
F4B
ρ
F5B
F8B
(b)
ρ (cm) SF Separation
14
12
10
8
6
4
2
Heat Flux
R (m)
1.38
1.34
1.30
1.26
MW/m2
0.0
0.4
0.8
1.2
1.6

Fig. 2

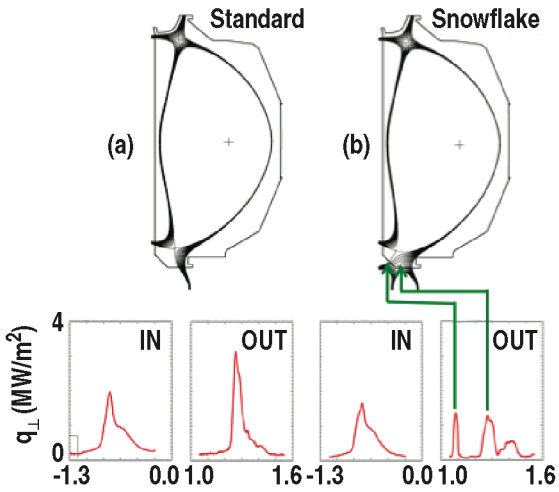
Standard
Snowflake
(a)
(b)
IN
OUT
IN
OUT
4
0
$q_\perp$ (MW/m^2)
-1.3
0.0
1.0
1.6
-1.3
0.0
1.0
1.6

Fig. 3

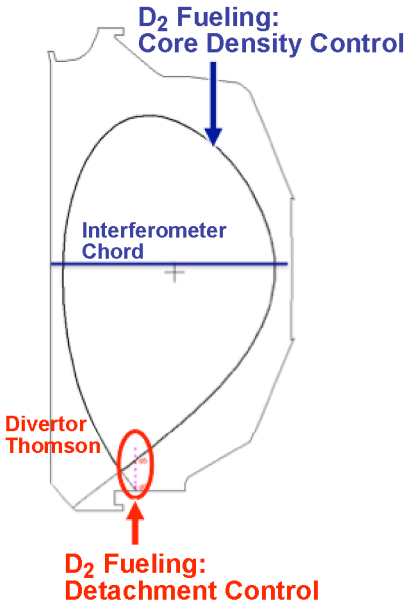
D_2 Fueling:
Core Density Control
Interferometer
Chord
Divertor
Thomson
D_2 Fueling:
Detachment Control

Fig. 4

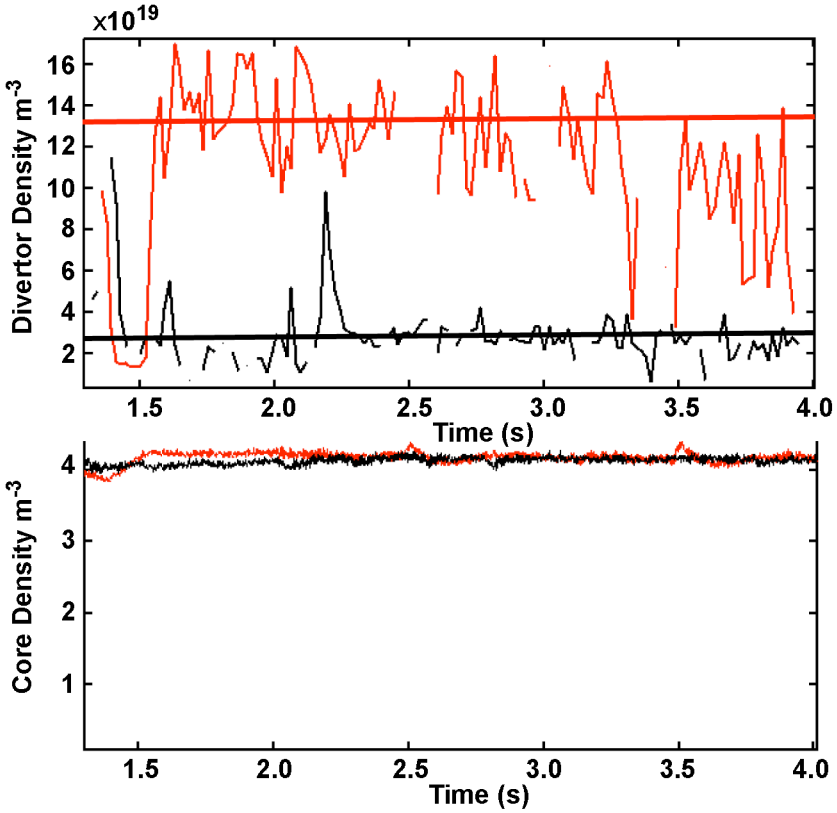
x10^19
Divertor Density m^-3
16
14
12
10
8
6
4
2
1.5
2.0
2.5
3.0
3.5
4.0
Time (s)
Core Density m^-3
4
3
2
1
1.5
2.0
2.5
3.0
3.5
4.0
Time (s)

Fig. 5

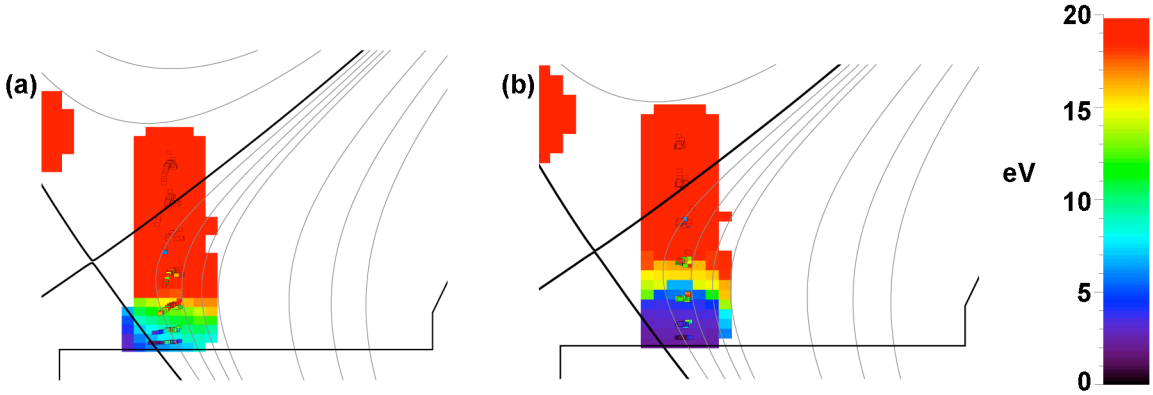

Fig. 6